An Input-to-State Safety Approach Toward Thermal Fault-Tolerant Battery Cells

Shashank Dhananjay Vyas, *Student Member, IEEE*, Tanushree Roy, *Member, IEEE,* and Satadru Dey, *Senior Member, IEEE*

***Abstract*—Lithium-ion battery cells remain susceptible to various forms of failures which originate from several sources including thermal abuse conditions. Many of these failures often result in thermal anomalies leading to runaway conditions. In order to address such critical issue, extensive research has been conducted on safer battery materials and mechanical designs. However, battery control systems can also play a crucial role in such endeavor. In this work, we focus on this issue and propose a thermal fault-tolerant control algorithm based on the notion of Input-to-State Safety which has garnered attention in various other safety-critical applications including robotics and automotive systems. The control design process utilizes a lumped parameter thermal model and Ordinary Differential Equation (ODE)-based practical input-to-state safety technique to formulate the thermal control problem. The design problem solves for control parameters using Barrier function and linear stability analysis. We present simulation studies to validate the proposed framework.**

***Index Terms*—Battery, Fault-tolerance, Input-to-State Safety, Thermal Fault.**

I. Introduction

In recent years, the presence of Lithium-ion (Li-ion) batteries has been significantly increased in electric vehicles and related transportation technologies, grid energy storage systems, and smart medical devices, among others. In spite of the appreciable growth in terms of energy density of Li-ion batteries, the safety of Li-ion batteries is still in need of urgent solutions. For example, a large number of cases of Li-ion battery failures have been reported which have resulted in hazardous occurrences such as smoke, explosions, fires [1]. Some of the the failures can be correlated to the chemical nature of Lithium. Since, lithium is a highly reactive element, it often results in the formation of conductive dendrites causing internal short circuits exacerbating the safety of Li-ion batteries [2]. In essence, owing to a booming Li-ion battery industry, considerable scope of improvement lies in the area of safety of Li-ion batteries. In this context, we propose a control algorithm for handling thermal faults in Li-ion battery cells, which can potentially boost safety under real-time operation.

This work was supported by National Science Foundation under Grant No. 2050315. The opinions, findings, and conclusions or recommendations expressed are those of the author(s) and do not necessarily reflect the views of the National Science Foundation.

S. Vyas and S. Dey are with the Department of Mechanical Engineering, The Pennsylvania State University, University Park, Pennsylvania 16802, USA. {sbv5192,skd5685}@psu.edu.

T. Roy is with the Department of Mechanical Engineering, Texas Tech University, Lubbock, Texas 79409, USA. tanushree.roy@ttu.edu.

A. Literature Review and Research Gaps

During the recent few years, the problem of fault detection and estimation in batteries has been studied extensively. For example in [3], detection of signature faults like over-charging and over-discharging is considered. Fault diagnosis and control of voltage and current sensors' is performed in [4] but thermal faults like thermal runaway are not considered which are the most common cause of Li-ion battery failures. Sensor data based approach is presented in [5] to detect thermal faults and predict temperature values. In [6], nonlinear observers are designed to construct residual signals which are then compared with adaptive thresholds for the detection of thermal faults.

Aforementioned works mostly focus on fault diagnostic issues in batteries. In terms of battery control, existing works typically fall into one of the following categories: charging control with a focus on optimal or fast charging [7], constraint management for performance improvement [8], [9], charge and thermal balancing [10]. Other than these categories, some thermal management approaches have also been presented [11]–[14]. However, these thermal control approaches do not consider control in the presence of battery faults. To ensure safety of batteries, control methods mitigating the effects of the faults are essential. There are some works in literature concerned with fault control techniques. A model predictive fault control framework is introduced at battery production level in [15] but do not consider control of batteries that are in-use. Review of some of the available literature on sensor fault tolerant control techniques for Li-ion batteries of electric vehicles has been presented in [16].

However, fault-tolerance under internal thermal faults (that is, faults that are not related to sensors but originated within the battery cells) has been significantly under-explored. In [17], a fault tolerant control scheme for internal thermal faults has been proposed. However, such approach falls into the category of active fault-tolerant control in the sense that it requires a real-time fault detector and estimator. Potential drawbacks of such active fault-tolerant control include [18]: (i) A real-time fault detector and estimator is needed. (ii) The effectiveness of the approach depends on accuracy of the fault detector and estimator. Any inaccuracy in the detector/estimator may induce delay in fault accommodation [18]. To avoid these drawbacks, we propose a passive fault-tolerant control algorithm leveraging ODE-based practical input-to-state safety technique. Such approach does not require a real-time fault detector and estimator.

B. Input-to-State Safety

The notion of input-to-state safety for ODE systems was introduced in [19]. Since then, Barrier function based technique has been explored in the literature [20]–[22] to analyze input-to-state safety. In [23] and [24], the notion of practical input-to-state safety was presented augmenting on the original notion. In this work, we adopt the approach presented in [23]. Specifically, the idea of input-to-state safety is enabled by a metric that computes the distance of the system states from a pre-defined unsafe region. The goal is to ensure that the distance metric is lower bounded by a combination of several terms related to initial condition and inputs [23]. This lower bound further ensures that the system states never enter the unsafe region. In our work, we adopt this technique to design the control algorithm such that the temperature states never enter the unsafe region even under the presence of faults.

C. Main Contributions

Keeping in mind the research gaps mentioned earlier, the main contribution of this paper is a passive fault-tolerant control algorithm to enable battery safety under thermal faults. In this algorithm, we formulate a control law which guarantees both the thermal safety and stability by combining lumped parameter battery cell thermal model and ODE-based practical input-to-state safety technique. Particularly, we design a control gain matrix such that battery temperatures get stabilized while remaining under the safe operating limits. In order to arrive at such design, a Barrier function based approach is used to devise the conditions to be satisfied by the control gain matrix such that temperatures never reach values beyond the safe range. Then the closed loop linear stability constraint is applied to the gains obtained from earlier conditions to keep the temperatures stable in the safe region.

A related work is presented in [25] where a Partial Differential Equation (PDE)-based input-to-state safety technique is applied to a battery module under thermal anomalies. The differences between the current work and [25] are as follows. (i) In [25], battery modules are considered which have large spatial temperature variation. Whereas the current work considers battery cells which do not have significant spatial temperature variation, so we utilize a lumped thermal model eliminating the need for complicated PDE analyses. (ii) Three sensors are considered in [25] for measurements, whereas only two sensors are considered in current work, thus achieving safety with limited sensing, and further reducing the implementation cost. (iii) We consider the coolant dynamics in our analysis which is not accounted for in [25].

A preliminary version of this work is published in [26]. This journal version extends the conference paper [26] by performing the following enhancements: (i) In terms of the models used, we have updated the battery thermal model to include the dynamics between control command and actuated cooling power. We have also included the cooling constraint as the upper limit of maximum cooling power. The conference version did not consider the aforementioned dynamics and the constraint on cooling power. (ii) In terms of control design, we have considered the dynamics between control command and actuated cooling power in the control design framework. We have also included the constraint on cooling power in the control design framework. Furthermore, we have added an additional safety consideration: we incorporated a safety upper bound on the thermal gradient between the core and the surface temperature of the battery. The conference version did not consider the aforementioned dynamics, the cooling power constraint, and the safety constraint on thermal gradient. These new additions make the final control design conditions slightly different, however, the overall structure of the design process remains the same. (iii) In terms of the simulation studies, we have used a high-fidelity distributed parameter thermal model as the plant dynamics to validate the proposed control approach in the journal version. In the conference version, we used the lumped parameter thermal model with zero mean Gaussian white noise as the plant dynamics. Furthermore, we have performed additional simulation case studies in the journal version: (a) independent faults in the core and surface of the battery cell, (b) coupled faults affecting both core and surface of the battery cell, (c) effect of measurement noise on the control performance, (d) effect of parametric uncertainties on the control performance. The conference version only had a case study with an independent core temperature fault, and no effect of uncertainties was studied.

D. Paper Organization

The organization of the rest of the paper is as follows: Section II describes the thermal model of the battery considered and discusses the problem statement. Section III explains the practical input-to-state safety based thermal control algorithm. Section IV shows the results from the simulation case studies. Section V concludes the paper.

TABLE I
MODEL VARIABLES AND PARAMETERS

Parameters/Varibales	Description	Unit
T_1	Core Temperature	K
T_2	Surface Temperature	K
T_∞	Ambient Temperature	K
$\dot{Q}$	Nominal Heat Generation	W
R_1	Conduction Resistance	KW^{-1}
R_2	Convection Resistance	KW^{-1}
C_1	Core Heat Capacity	JK^{-1}
C_2	Surface Heat Capacity	JK^{-1}
I	Current through Battery	A
Q_b	Battery capacity	As
V_{ocv}	Battery Open Circuit Voltage	V
V_t	Battery Terminal Voltage	V
C_∞	Cooling System Heat Capacity	JK^{-1}
$\dot{Q}_p$	Actual Cooling System Power	W
$\dot{Q}_c$	Commanded Cooling System Power	W
τ_c	Cooling System Time Constant	s

II. MATHEMATICAL MODELS

First, we describe the mathematical models utilized in this work. The variables and parameters of the model are described in Table I.

1) Battery thermal dynamics: We consider a cylindrical battery cell in this work, which can be described by a lumped parameter thermal model for cylindrical battery cells from [27], [28]:

$$\dot{T}_1(t) = -\frac{T_1(t) - T_2(t)}{R_1 C_1} + \frac{\dot{Q}(t)}{C_1}, \tag{1}$$

$$\dot{T}_2(t) = -\frac{T_2(t) - T_1(t)}{R_1 C_2} - \frac{T_2(t) - T_\infty(t)}{R_2 C_2}, \tag{2}$$

where the parameters are given below.

2) Battery electrical dynamics: Since the heat generation term in battery thermal model depends on battery electrical behavior, we adopt an electrical model described by two parts [29]: (i) State-of-Charge (SOC) dynamics captured by Coulomb counting, and (ii) terminal voltage captured by an open circuit voltage and electrical resistor (R) in series. This model is based on widely used equivalent circuit modeling approach - a review of such equivalent circuit models can be found in [30]. The modeling equations are given by:

$$\dot{SOC}(t) = -\frac{I(t)}{Q_b}, \tag{3}$$

$$V_t(t) = V_{ocv}(SOC) - I(t)R_s. \tag{4}$$

Then we adopt the following heat generation model proposed in [31]:

$$\dot{Q}(t) = I(t)\left(V_{ocv}(SOC) - V_t(t) - T_1(t)\frac{d(OCV)}{dT}\right), \tag{5}$$

where $\frac{dOCV}{dT}$ is the entropic heat coefficient. Rearranging the terms of (5), we write:

$$\dot{Q}(t) = R_s u_1^2(t) - \alpha u_1(t) T_1(t), \tag{6}$$

where $R_s u_1^2(t)$ is the approximation of the term $I(t)(V_{ocv}(SOC) - V_t(t))$ with $u_1(t) = I(t)$; and $\alpha = \frac{d(OCV)}{dT}$.

3) Battery cooling dynamics: Next, the cooling system dynamics is considered as [17]:

$$\dot{T}_\infty(t) = -\frac{T_\infty(t) - T_2(t)}{R_2 C_\infty} - \frac{Q_p(t)}{C_\infty}, \tag{7}$$

$$\tau_c \dot{Q}_p(t) = -Q_p(t) + Q_c(t), \tag{8}$$

where the parameters are given below. This model is based on liquid cooling where we control Q_c by changing the flow rate of the coolant. Note that the first order dynamics (8) capture the delay between control command and cooling system actuation through the time constant τ_c.

4) Battery thermal fault dynamics: We model the faults as unknown additive terms acting on the core and surface of the battery cell [6]. Under this modeling assumption, battery thermal model (1)-(2) becomes:

$$\dot{T}_1(t) = -\frac{T_1(t) - T_2(t)}{R_1 C_1} + \frac{\dot{Q}(t)}{C_1} + \frac{f_1(t)}{C_1}, \tag{9}$$

$$\dot{T}_2(t) = -\frac{T_2(t) - T_1(t)}{R_1 C_2} - \frac{T_2(t) - T_\infty(t)}{R_2 C_2} + \frac{f_2(t)}{C_2}, \tag{10}$$

where $f_1(t)$ and $f_2(t)$ are the thermal faults which may occur due to unwanted chemical reactions, abnormal heat generation inside the battery or mechanical disruptions [32]–[34].

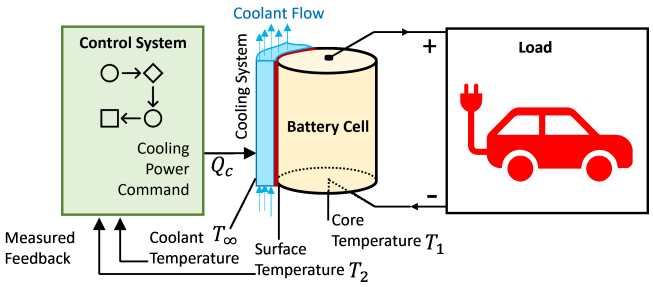

Fig. 1. Conceptual schematic of the thermal control system.

III. Practical Input-to-State Safety based Control Design

In this section, we describe the control design to achieve thermal fault-tolerance. A schematic representation of the control framework is shown in Fig. 1. We assume that the surface temperature of the battery cell and the cooling temperature are measured and used as feedback information to the control algorithm. Before deriving the control algorithm, we formulate the state-space model of the battery system considering (7), (8), (9), and (10). Considering $X = [T_1, T_2, T_\infty, Q_p]^{'}$ as the state vector, $u_1 = I$ as current, $u_2 = Q_c$ as the control input, $\Delta = [f_1, f_2]^{'}$ as the fault vector, and $y = [T_2, T_\infty]^{'}$ as the output vector, the state-space model takes the following form:

$$\dot{X} = (A_0 + A_1(u_1))X + B_1 u_1^2 + B_2 u_2 + F\Delta, \tag{11}$$

$$y = CX, \tag{12}$$

where

$$A_0 = \begin{bmatrix} -\frac{1}{C_1 R_1} & \frac{1}{C_1 R_1} & 0 & 0 \\ \frac{1}{C_2 R_1} & -\frac{1}{C_2}(\frac{1}{R_1} + \frac{1}{R_2}) & \frac{1}{C_2 R_2} & 0 \\ 0 & \frac{1}{C_\infty R_2} & -\frac{1}{C_\infty R_2} & -\frac{1}{C_\infty} \\ 0 & 0 & 0 & -\frac{1}{\tau_c} \end{bmatrix}, \tag{13a}$$

$$A_1(I) = \begin{bmatrix} -\frac{\alpha I}{C_1} & 0 & 0 & 0 \\ 0 & 0 & 0 & 0 \\ 0 & 0 & 0 & 0 \\ 0 & 0 & 0 & 0 \end{bmatrix}, \quad B_1 = \begin{bmatrix} \frac{R_s}{C_1} \\ 0 \\ 0 \\ 0 \end{bmatrix}, \tag{13b}$$

$$B_2 = \begin{bmatrix} 0 \\ 0 \\ 0 \\ \frac{1}{\tau_c} \end{bmatrix}, \; F = \begin{bmatrix} \frac{1}{C_1} & 0 \\ 0 & \frac{1}{C_2} \\ 0 & 0 \\ 0 & 0 \end{bmatrix}, \; C = \begin{bmatrix} 0 & 1 & 0 & 0 \\ 0 & 0 & 1 & 0 \end{bmatrix}. \tag{13c}$$

Remark 1: Note that we consider only cooling power (Q_p) as the control input and not the current (I). Although the battery current is typically measured and hence, a known variable to the controller, oftentimes the current is determined to satisfy the power demand from the battery. For example, in vehicles, current drawn depends on the action of the driver. Under such scenarios, the current is not manipulated by the thermal control unit and cooling power remains the only control variable. Nevertheless, if the current (I) is also allowed to be manipulated as a control input by the thermal management system, the temperature control logic can be modified to reduce the additional heat generation effect by

restricting the current drawn from or fed to the battery. An example control logic is stated as follows: If the measured surface and/or coolant temperature reach close to the unsafe region, then in addition to changing the value of cooling power (Q_p), the current (I) can also be reduced to a lower value resulting in lower heat generation. This in turn leads to controlling the temperature rise. Such a logic based restriction on charge or discharge can also be implemented if the fault is too high such that the coolant power has reached its critical value and is unable to decrease the battery temperature further. This control logic can be easily augmented to the proposed input-to-state safety based cooling control as a safety filter without making any significant changes in our design.

Remark 2: In the problem formulation, the fault appears to be independent of the battery current input u_1, but it is to be noted that u_1 can indeed have an impact on the thermal fault. For example, it might lead to additional current component resulting in the net current as $u_1 + \Delta_{u1}$. The effect of such an impact will be manifested in the form of additional heat generation $\delta\dot{Q}$, and the net heat generation will be $\dot{Q} + \delta\dot{Q}$ where $\dot{Q}$ is given by (6) and $\delta\dot{Q} = R_s\Delta_{u1}^2(t) + 2R_s u_1(t)\Delta_{u1}(t) - \alpha\Delta_{u1}(t)T_1(t)$. This results in core temperature dynamics given by (9) to get modified as follows,

$$\dot{T}_1(t) = -\frac{T_1(t) - T_2(t)}{R_1 C_1} + \frac{\dot{Q}(t)}{C_1} + \frac{\delta\dot{Q}(t)}{C_1} + \frac{f_1(t)}{C_1}. \quad (14)$$

which can be further written as,

$$\dot{T}_1(t) = -\frac{T_1(t) - T_2(t)}{R_1 C_1} + \frac{\dot{Q}(t)}{C_1} + \frac{\tilde{f}_1(t)}{C_1}, \quad (15)$$

where $\tilde{f}_1(t) = f_1(t) + \delta\dot{Q}(t)$. Thus, for fault in current u_1 we can re-write the battery model (11) with the new fault term written as $\Delta = [\tilde{f}_1, f_2]'$. Consequently, it is evident that our design methodology can be easily extended to detect such faults which modify current u_1 as well.

Remark 3: In this work, we have modeled the thermal faults as an additive component to the nominal temperature model. This standard form of representation of thermal faults has been an accepted practice in the existing literature [6], [17], [35]–[37]. It is possible to have different root causes for battery faults [32], [33], however, a majority of them ultimately manifest themselves as abnormal heat generation in excess to nominal heat. Furthermore, such additive representation aids the analysis and synthesis of the input-to-state safety based control. Finally, as described in Remark 2, we are not making any assumption on the origin of the thermal fault. It can be potentially temperature and/or current dependent. This justifies our adopted approach.

Next, based on the above state-space model formulation, the control objectives is to achieve the following:

- **Thermal Safety:** Ensure the temperatures do not reach any value in a pre-defined unsafe operating range during its operation, even in the presence of faults.
- **Thermal Stability:** Keep the closed-loop temperature dynamics stable.
- **Thermal Performance:** Ensure the temperatures are around some pre-determined reference values under nominal conditions.

However, the control performance is subject to the limits of cooling power, described by

$$Q_p \leq \bar{Q}_p, \quad (16)$$

where $\bar{Q}_p$ is the maximum feasible cooling power. To attain the above control objectives, we aim to design a feedback control law of the following form:

$$u_2 = -KC(X - X_{ref}), \quad (17)$$

where $K = \begin{bmatrix} K_2 & K_3 \end{bmatrix}$ is the control gain matrix. We take $X_{ref} = [T_{1,ref}, T_{2,ref}, T_{\infty,ref}, 0]'$ as the reference steady state vector such that $T_i \to T_{i,ref}$ as $t \to \infty$ for $i = 1, 2, 3$. Next, we apply a change of variables given by $\xi = X - X_{ref}$ in (11), and subsequently use (17) to obtain:

$$\dot{\xi} = (P + A_1(u_1))\xi + B_1 u_1^2 + (P + A_1(u_1))X_{ref} + F\Delta, \quad (18)$$

where $P = A_0 - B_2 KC$. In the next section, we discuss the details of the control gain design. Next, we will discuss the notion of Input-to-State Safety which will be used to achieve the aforementioned control objectives.

A. Basics of Practical Input-to-State Safety

The notion of input-to-state safety essentially formulates inequality type conditions to ensure the system states are within safe operating region [23]. Adopting and slightly modifying the definition presented in [23], and considering a system with state ξ and denoting the distance of the state from a pre-defined unsafe set $\mathbb{D}$ as $|\xi|_{\mathbb{D}}$, we can write the practical input-to-state safety condition as:

$$|\xi|_{\mathbb{D}} \geq \alpha_1(|\xi(0)|_{\mathbb{D}}, t) - \alpha_2(\|\delta\|, t) - \alpha_3, \ \forall t > 0. \quad (19)$$

In the above definition, the term δ captures the effects of uncontrolled inputs, which are u_1 and Δ in the context of battery thermal control problem; the functions are α_1, α_2 are class $\mathcal{KK}$ functions [23], and $\alpha_3 > 0$.

In our context, the notion of input-to-state safety should be interpreted as *maintain states within safe set under anomalous inputs*. This is enabled by defining a distance metric which tracks the distance between system state and unsafe region. Such distance is affected mainly by two competing terms: one arising from system initial conditions and another one arising from the effects of anomalous input. The idea behind the input-to-state safety definition is as follows: The distance of the system state from the unsafe set is mainly governed by the initial distance and the effect of uncontrolled inputs. The anomalous and uncontrolled inputs can potentially make the distance to be zero by bringing the states into the unsafe set. Under this scenario, the system is said to be practically input-to-state safe if the distance for all time is positive. The *practical* aspect is captured by the parameter α_3 which accounts for various forms of uncertainties. In the control design, our goal will be to find the control gains such that the safety distance is always positive.

Based on the above notion, we can characterize such practical input-to-state safety using Barrier functions [23]. The idea behind the construction of these Barrier functions is similar to that of Lyapunov function for control. Specifically, using the Barrier function we design a control input which enforces the system to remain within the safe set, if it started within the safe set. In other words, a system is defined to be safe, if the safe set remains forward invariant. Therefore, the continuously differentiable Barrier functions are chosen such that their superlevel set defines the boundary of the safe set. Additionally, to ensure the forward invariance of the safe set, the Barrier function is chosen such that it remains non-positive for trajectories within safe set and the control input is designed such that its rate of change along the trajectory also remains non-positive. Now, in the presence of disturbances and uncontrollable inputs, the Barrier function can provide theoretical guarantees on the allowable upper bound for these disturbances and inputs for which the designed control policy will ensure system's safety. We also note here that the above conditions on the Barrier functionals are generally easier to formulate if the Barrier function is defined explicitly in terms of the distance of the state trajectory from unsafe set instead of the system state itself.

Under this characterization, our objective is to find a Barrier function $\mathbb{B}\colon \mathbb{R}^3\backslash\mathbb{D} \rightarrow \mathbb{R}$, which satisfies the following inequalities [23], [25]:

$$-c_1|\xi|_{\mathbb{D}}^2 - \kappa_1 \leqslant \mathbb{B}(\xi) \leqslant -c_2|\xi|_{\mathbb{D}}^2, \tag{20}$$

$$\dot{\mathbb{B}}(\xi) \leqslant -c_3|\xi|_{\mathbb{D}}^2 + c_4\left|u_1\right|^2 + c_5\left\|\Delta\right\|^2 + \kappa_2, \tag{21}$$

where $c_i > 0,\ i = 1,2,3,4,5;\ \kappa_i \geqslant 0,\ i = 1,2$, and $\|.\|$ indicates the 2-norm. Notably, condition (20) here establishes the non-positivity of the Barrier functional within the safe set $\mathbb{D}^C = \mathbb{R}^3\backslash\mathbb{D}$. Similarly, condition (21) ensures that the designed control policy will guarantee the trajectories to stay within the safe set, depending on the maximum allowable norm of the disturbance input δ, current input u_1, and some constant κ_2 (included to facilitate some practical design flexibility). Thus, these conditions (20)-(21) implies that the safe set $\mathbb{D}^C$ remains forward invariant for the system for some allowable disturbances and inputs under a designed control policy. This consequently implies that the system is practically input-to-state safe with respect to the unsafe set $\mathbb{D}$ for some norm-bounded disturbances δ, input signal u_1, and design constant κ_2. As mentioned before, we note that $|\xi|_{\mathbb{D}}$ is the distance of system states from the unsafe set, and not the actual states of the system.

Remark 4: Note that since the conditions on control gains are dependent on Barrier function, as is evident in the next subsection, the form of Barrier function chosen naturally affects the design. To allow a quadratic form of Barrier function for design, κ_1 ensures that $\mathbb{B}(\xi)$ can be lower bounded on the boundary of unsafe region since $|\xi|_{\mathbb{D}} = 0$ on the boundary [23]. Moreover, the effect of other system and design parameters such as the reference state values and the maximum allowable state values are captured in the parameter κ_2.

B. Thermal Fault-tolerant Control Design Process

To this end, our goal is to design the control parameter K in (17). Note that the control goal is to be away from the unsafe set while not to deviate too far from the reference state $X_{ref} = [T_{1,ref}, T_{2,ref}, T_{\infty,ref}, 0]'$ where $T_{1,ref}, T_{2,ref}, T_{\infty,ref}$ are the reference temperatures for the core, surface and the coolant, respectively. In order to apply the practical input-to-state safety technique, we first focus on defining an unsafe set through the following conditions:

- Core temperature should be within certain pre-defined upper bound, i.e. $T_1 \approx T_{1,ref} < \overline{T}_1$.
- Surface temperature should be within certain pre-defined upper bound, i.e. $T_2 \approx T_{2,ref} < \overline{T}_2$.
- Temperature gradient between the core and surface should be within certain pre-determined limit, i.e. $|T_1 - T_2| < \delta$.
- Coolant temperature should be within certain pre-defined upper bound, i.e. $T_\infty \approx T_{\infty,ref} < \overline{T}_3$.
- Coolant temperature should be within certain pre-defined upper bound, i.e. $Q_p \approx 0 < \overline{Q}_p$.

Here, we define upper bounds of the temperature states are $\overline{T}_1$, $\overline{T}_2$, and $\overline{T}_3$, and δ is the limit beyond which the difference between core and surface temperatures should not exceed. If the temperatures violate these bounds, it will be considered unsafe condition. On the other hand, if the cooling power required rises beyond the limit, it will be considered as infeasible control.

Remark 5: Note that the first three conditions are essentially the true safety conditions. The fourth and fifth conditions are essentially actuation limitation constraints. In order to maintain safety within this cooling constraint, and to enable the application of input-to-state safety technique, we add all of them together as safety conditions.

Based on these bounds, we define the following unsafe set:

$$\mathbb{D} = \{a = [a_1, a_2, a_3, a_4]^{'} : (a_1^2 + a_2^2 + a_3^2 + a_4^2) > \mathcal{M}^2, \\ |a_1 - a_2| > \delta\}, \tag{22}$$

where

$$\mathcal{M} := \min\Big(w_1\left(\overline{T}_1 - T_{1,ref}\right), w_2\left(\overline{T}_2 - T_{2,ref}\right), \\ w_3\left(\overline{T}_3 - T_{3,ref}\right), w_4\overline{Q}_p, w_5\frac{\delta}{2}\Big), \tag{23}$$

with w_i for $i = 1, 2, ..., 5$ being the weighting factors. We have chosen the weighting factors as $w_i = 1$ for $i = 1, 2, ..., 5$.

1) Unsafe set geometric representation: The unsafe set $\mathbb{D}$ represents a 4-dimensional (4D) hyper-sphere. $\mathcal{M}$ represents the radius of the hyper-sphere. For simpler visualization, we show a 2-dimensional (2D) conceptualization of the unsafe set in Fig. 2 to illustrate the approach. The blue coloured regions in Fig. 2(a), (b) and (c) refer to the safe set whose boundary is red in colour. Any point lying outside the blue region falls in the unsafe set. The 2D representation is essentially a projection of the 4D hyper-sphere on the the plane of ξ_1 and ξ_2. For simplicity, we choose $T_{1,ref} = T_{2,ref}$ resulting in $|\xi_1 - \xi_2| = |T_1 - T_2|$ so that in Fig. 2, $|T_1 - T_2| < \delta$ is equivalent to $|\xi_1 - \xi_2| < \delta$. Further in Fig. 2 we have shown three different

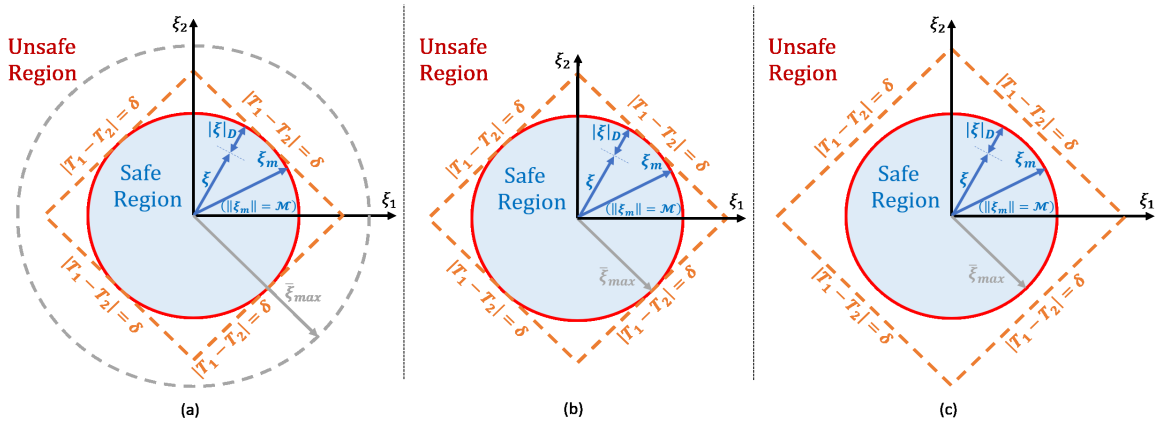

Fig. 2. A visual representation of safe and unsafe regions as projected in 2 dimensions for (a) $\mathcal{M} = \frac{\delta}{2} < \xi_{max}$, (b) $\mathcal{M} = \frac{\delta}{2} = \xi_{max}$ and (c) $\mathcal{M} = \xi_{max} < \frac{\delta}{2}$, where $\mathcal{M}$ is given by (23) and $\xi_{max} = min\left(\overline{T_1} - T_{1,ref}, \overline{T_2} - T_{2,ref}\right)$.

cases where $\xi_{max} = min\left(\overline{T_1} - T_{1,ref}, \overline{T_2} - T_{2,ref}\right)$. First, Fig. 2(a) corresponds to the case where the temperature difference $|T_1 - T_2| < \delta$ is the limiting condition for the radius of the hyper-sphere resulting in $\mathcal{M} = \frac{\delta}{2} < \xi_{max}$. Second, Fig. 2(b) corresponds to the case where the temperature difference $|T_1 - T_2| < \delta$ and the maximum allowable temperatures $T_1 < \overline{T}_1$, $T_2 < \overline{T}_2$ are equivalent limiting conditions for the radius of the hyper-sphere resulting in $\mathcal{M} = \frac{\delta}{2} = \xi_{max}$. Third, Fig. 2(c) corresponds to the case where the maximum allowable temperatures $T_1 < \overline{T}_1$, $T_2 < \overline{T}_2$ are the limiting conditions for the radius of the hyper-sphere resulting in $\mathcal{M} = \xi_{max} < \frac{\delta}{2}$.

2) Distance metric definition: Next, we define a metric for the distance of the states ξ with respect to the unsafe set $\mathbb{D}$ as follows:

$$|\xi|_{\mathbb{D}} = \inf_{a \in \mathbb{D}} \|\xi - a\|, \tag{24}$$

where $\mathbb{D}$ is given by (22). Qualitatively, $|\xi|_{\mathbb{D}}$, which is the 2-norm of $(\xi - a), \forall a \in \mathbb{D}$, represents the minimum distance of the state ξ from the unsafe set $\mathbb{D}$. This essentially implies

$$|\xi|_{\mathbb{D}} = \mathcal{M} - \|\xi\|, \quad \forall \xi \in \mathbb{S} = \mathbb{D}^C, \tag{25}$$

where $\mathbb{S}$ is the safe set, that is, the complement of the unsafe set $\mathbb{D}$.

3) Safety using Barrier function: Next, we choose the following Barrier function candidate:

$$\mathbb{B}(\xi) = \|\xi\|^2 - \mathcal{M}^2, \tag{26}$$

where $\mathcal{M}$ is defined in (23).

In order to obtain the left-hand side inequality of (20), we use (25) in the definition of (26) obtaining $\mathbb{B}(\xi) = -|\xi|_D^2 - 2|\xi|_D \|\xi\|$. Further we not from (25) that $|\xi|_D, \|\xi\| \leqslant \mathcal{M}$ which yields,

$$-c_1|\xi|_{\mathbb{D}}^2 - \kappa_1 \leqslant \mathbb{B}(\xi), \tag{27}$$

where $c_1 = 1$ and $\kappa_1 = 2\mathcal{M}^2$. This provides us with the left-hand side inequality of (20).

Next to obtain the right-hand side inequality of (20), we rearrange the terms in (26) to obtain, $\mathbb{B}(\xi) = -(\mathcal{M} - \|\xi\|)^2 - 2\|\xi\|(\mathcal{M} - \|\xi\|)$. Since $\|\xi\| < \mathcal{M}$, it can be seen that $\mathbb{B}(\xi) \leqslant -(\mathcal{M} - \|\xi\|)^2$. From Fig. 2, it is evident that $|\xi|_{\mathbb{D}} = (\mathcal{M} - \|\xi\|)$. This implies that,

$$\mathbb{B}(\xi) \leqslant -c_2|\xi|_{\mathbb{D}}^2, \tag{28}$$

where $c_2 = 1$. This provides us with the right-hand side inequality of (20).

Next, we find the condition for which (21) is satisfied. Let $\xi_m = [\xi_{1m}, \xi_{2m}, \xi_{3m}, \xi_{4m}]'$ represent any point on the boundary of the safe set $\mathbb{S}$ which implies

$$\|\xi_m\| = \mathcal{M}. \tag{29}$$

Noting $\|\xi\|^2 = \xi'\xi$, we rewrite (26) as $\mathbb{B}(\xi) = \xi'\xi - \mathcal{M}^2$. Differentiation of which yields $\dot{\mathbb{B}}(\xi) = 2\xi'\dot{\xi}$ which can be written as $\dot{\mathbb{B}}(\xi) = 2(\xi - \xi_m + \xi_m)'\dot{\xi}$ and further substituting $\dot{\xi}$ from (18), we obtain,

$$\dot{\mathbb{B}} = V_0 + V_1 + V_2 + V_3 + V_4 + V_5, \tag{30}$$

where

$$V_0 = (\xi - \xi_m)'P(\xi - \xi_m) + (\xi - \xi_m)'(2P\xi_m + PX_{ref}), \tag{31}$$

$$V_1 = -\frac{\alpha(\xi_1 - \xi_{1m})^2 u_1}{C_1} + \frac{R_s(\xi_1 - \xi_{1m})u_1^2}{C_1} - \frac{2\alpha(\xi_{1m} + \frac{T_{1,ref}}{2})(\xi_1 - \xi_{1m})u_1}{C_1}, \tag{32}$$

$$V_2 = -\frac{\alpha\xi_{1m}(\xi_{1m} + T_{1,ref})u_1}{C_1} + \frac{R_s\xi_{1m}u_1^2}{C_1}, \tag{33}$$

$$V_3 = \frac{(\xi_1 - \xi_{1m})f_1}{C_1} + \frac{(\xi_2 - \xi_{2m})f_2}{C_2}, \tag{34}$$

$$V_4 = \frac{\xi_{1m}f_1}{C_1} + \frac{\xi_{2m}f_2}{C_2}, \tag{35}$$

$$V_5 = \xi_m'P\xi_m + \xi_m'PX_{ref}. \tag{36}$$

Next, we make use of the Holder's and then Young's inequality of the form

$$xy \leqslant \|x\|\|y\| \leqslant \frac{\bar{\gamma}}{2}\|x\|^2 + \frac{1}{2\bar{\gamma}}\|y\|^2, \ \bar{\gamma} > 0, \tag{37}$$

on (31) through (36). Furthermore, denoting $(\xi - \xi_m)$ by $\hat{\xi}$; $(\xi_1 - \xi_{1m})$ by $\hat{\xi_1}$; $(\xi_2 - \xi_{2m})$ by $\hat{\xi}_2$, we obtain the following upper bounds from (31)-(36):

$$V_0 \leqslant \hat{\xi}^{'} P \hat{\xi} + \gamma_1 \left\|\hat{\xi}\right\|^2 + \frac{\left\|2P\xi_m + PX_{ref}\right\|^2}{4\gamma_1}, \tag{38}$$

$$V_1 \leqslant \alpha\hat{\xi_1^2} + \gamma_2 u_1^2 + \frac{1}{4\gamma_2 C_1^2} + \gamma_3\hat{\xi_1^2} + \frac{1}{4\gamma_3} + \frac{R_s}{C_1}u_1^2 + \gamma_4\hat{\xi_1^2} + \frac{\alpha^2(2\xi_{1m} + T_{1,ref})^2}{4\gamma_4 C_1^2}u_1^2, \tag{39}$$

$$V_2 \leqslant \gamma_5 u_1^2 + \frac{\alpha^2\xi_{1m}^2(\xi_{1m} + T_{1,ref})^2}{4\gamma_5 C_1^2} + \frac{R_s\xi_{1m}}{C_1}u_1^2, \tag{40}$$

$$V_3 \leqslant \gamma_6\hat{\xi_1^2} + \frac{1}{4\gamma_6 C_1^2}f_1^2 + \gamma_7\hat{\xi_2^2} + \frac{1}{4\gamma_7 C_2^2}f_2^2, \tag{41}$$

$$V_4 \leqslant \gamma_8 f_1^2 + \frac{\xi_{1m}^2}{4\gamma_8 C_1^2} + \gamma_9 f_2^2 + \frac{\xi_{2m}^2}{4\gamma_9 C_2^2}, \tag{42}$$

where $\gamma_i > 0,\ i = 1, 2, ..., 9$. Next, using the fact that $\hat{\xi_1^2} \leqslant \left\|\hat{\xi}\right\|^2$, $f_1^2 \leqslant \|\Delta\|^2$ and $f_2^2 \leqslant \|\Delta\|^2$ in (39), (41), (42), and then using (36)-(42) in (30), we obtain,

$$\dot{\mathbb{B}} \ \leqslant \ \hat{\xi}^{'} P \hat{\xi} \ + \ \gamma \left\|\hat{\xi}\right\|^2 \ + \ c_4 u_1^2 \ + \ c_5 \left\|\Delta\right\|^2 \ + \ \kappa_2, \tag{43}$$

where $\gamma = \gamma_1 + \alpha + \gamma_3 + \gamma_4 + \gamma_6 + \gamma_7$, and

$$c_4 = \gamma_2 + \frac{R_s}{C_1} + \frac{\alpha^2(2\xi_{1m} + T_{1,ref})^2}{4\gamma_4 C_1^2} + \gamma_5 + \frac{R_s\xi_{1m}}{C_1}, \tag{44}$$

$$c_5 = \frac{1}{4\gamma_6 C_1^2} + \frac{1}{4\gamma_7 C_2^2} + \gamma_8 + \gamma_9, \tag{45}$$

$$\kappa_2 = \frac{\left\|2P\xi_m + PX_{ref}\right\|^2}{4\gamma_1} + \frac{1}{4\gamma_2 C_1^2} + \frac{1}{4\gamma_3} + \frac{\alpha^2\xi_{1m}^2(\xi_{1m} + T_{1,ref})^2}{4\gamma_5 C_1^2} + \frac{\xi_{1m}^2}{4\gamma_8 C_1^2} + \frac{\xi_{2m}^2}{4\gamma_9 C_2^2} + \xi_m^{'} P\xi_m + \xi_m^{'} PX_{ref}. \tag{46}$$

Noting $\left\|\hat{\xi}\right\|^2 = \hat{\xi}^{'}\hat{\xi}$, we rewrite (43) as,

$$\dot{\mathbb{B}} \leqslant -\hat{\xi}^{'} R \hat{\xi} + c_4 u_1^2 + c_5 \left\|\Delta\right\|^2 + \kappa_2, \tag{47}$$

where $R = -(P + \gamma\mathbb{I})$ should be designed to be a positive definite matrix with $\mathbb{I}$ being the 4x4 identity matrix.

Given $R > 0$, we can write

$$\lambda_{min}(R)\left\|\hat{\xi}\right\|^2 \leqslant \hat{\xi}^{'} R \hat{\xi} \leqslant \lambda_{max}(R)\left\|\hat{\xi}\right\|^2, \tag{48}$$

where $\lambda_{min}(R)$ and $\lambda_{max}(R)$ be the minimum and maximum eigenvalues of R respectively. Furthermore, since $\hat{\xi} = (\xi - \xi_m)$ is as defined after (37), $\hat{\xi}$ represents a vector inside the safe set drawn from the state to the safe set boundary. But the length of this vector is always greater than or equal to the minimum distance of the state from the safe set boundary given by (25). Hence, we can write $|\xi|_{\mathbb{D}} \leqslant \|\xi - \xi_m\|$ giving $-\|\xi - \xi_m\|^2 \leqslant -|\xi|_{\mathbb{D}}^2$. This essentially implies we can write (47) as,

$$\dot{\mathbb{B}} \leqslant -c_3|\xi|_{\mathbb{D}}^2 + c_4 u_1^2 + c_5\left\|\Delta\right\|^2 + \kappa_2, \tag{49}$$

where $c_3 = \lambda_{min}(R)$.

Remark 6: From the design viewpoint, our goal is to ensure that $R = -(P + \gamma\mathbb{I})$ as defined after (47), should be a positive definite matrix. As $P = A_0 - B_2KC$, we find the control gain matrix K such that this condition is satisfied. Since $\gamma_i > 0,\ i \in \{1, 2, \ldots, 9\}$, it can be seen that $c_4 > 0$ and $c_5 > 0$ as defined in (44) and (45). To ensure that c_3 defined after (49) is positive, it is sufficient to ensure that $R > 0$. Further ensuring $\kappa_2 > 0$ provides us with the inequality condition (21). Satisfying these conditions essentially makes the system practically input-to-state stable in the sense of (20)-(21).

Note that the system (18) should also be closed-loop stable, according to the second control objective. Hence, the control gain matrix K should further ensure that the closed loop temperature dynamics is stable, i.e., all the eigenvalues of $(P + A_1(I))$ should have negative real part for the range of possible currents $I_{min} \leqslant I \leqslant I_{max}$ where I_{min} and I_{max} are the minimum and maximum values of allowable currents, respectively. Let $\lambda_i,\ \mathrm{i} \in \{1, 2, 3, 4\}$ be the eigenvalues of $(P + A_1(I))$, then the stability condition is as follows,

$$\text{real}(\lambda_i) < 0,\ i \in \{1, 2, 3, 4\}, \quad \forall \quad I \in [I_{min}, I_{max}]. \tag{50}$$

C. Summary of Control Design

In summary, the control design that ensures the practical input-to-state safety inequalities and stability condition, should satisfy the following:

$$-(P + \gamma\mathbb{I}) > 0, \tag{51}$$

$$\kappa_2 > 0, \tag{52}$$

$$\text{real}(\lambda_i) < 0,\ i \in \{1, 2, 3, 4\}, \forall I \in [I_{min}, I_{max}], \tag{53}$$

where P, γ and $\mathbb{I}$ are defined after (18), (43) and (47), respectively; κ_2 is given by (46); and $\lambda_i,\ \mathrm{i} = 1, 2, 3, 4$ are the eigenvalues of $(P + A_1(I))$.

IV. Results and Discussion

In this section, we test the proposed control framework using simulation case studies. First, we proceed with discussing the *plant model* used for testing purposes and then we state the simulation conditions.

A. Plant Model for Validation

The model (7), (8), (9), and (10), based on which the control design is performed, is formed on lumped modeling assumptions. However, in reality, the temperature within the battery cell is spatially distributed. In our testing, we consider a distributed parameter temperature dynamics to capture more realistic scenarios. This will also help understand the effectiveness of the proposed control approach when there are unmodelled dynamics. To this end, we consider the following distributed parameter thermal model (captured by a Partial Differential Equation (PDE)) as the plant dynamics [38]:

$$\frac{\partial T_p}{\partial t} = \frac{k}{\rho C_p}\frac{\partial^2 T_p}{\partial r^2} + \frac{k}{\rho C_p r}\frac{\partial T_p}{\partial r} + \frac{1}{\rho C_p}\frac{\dot{Q}}{V_{cell}}, \tag{54}$$

$$\frac{\partial T_p}{\partial t}\Big|_{r=0} = 0,\ \frac{\partial T_p}{\partial t}\Big|_{r=R} = -\frac{h}{k}(T_p(R) - T_\infty), \tag{55}$$

where $T_p(r,t)$ is the radially distributed temperature of the battery cell. In this plant dynamics, we have augmented the cooling dynamics (7) and (8) to complete the system of equations. Definitions of the plant model parameters are given in Table II. We have used this model to generate the feedback measurements to be used by the control algorithm. Subsequently, we performed parameter identification process to find the design model parameters that provides best fit with the plant model responses. The model fitting outcome is shown in Fig. 3 under a specific cooling condition, with resulting parameters given in Table III.

TABLE II
PLANT MODEL PARAMETERS

Parameter	Description	Unit
T_∞	Ambient Temperature	K
k	Battery Thermal Conductivity	$Wm^{-1}K^{-1}$
ρ	Battery Mass Density	kgm^{-3}
C_p	Specific Heat Capacity	$Jkg^{-1}K^{-1}$
h	Convection Coefficient	$Wm^{-2}K^{-1}$
R	Radius	m
$\dot{Q}$	Heat Generation	W

TABLE III
PARAMETER VALUES OF PDE PLANT MODEL AND ODE DESIGN MODEL

Parameter	Value
k	1.7999 $Wm^{-1}K^{-1}$
ρ	2.75x10^{-3} kgm^{-3}
C_p	1250 $Jkg^{-1}K^{-1}$
h	50 $Wm^{-2}K^{-1}$
R	9.15x10^{-3} m
R_1	2.64 KW^{-1}
R_2	3.46 KW^{-1}
C_1	51.9 JK^{-1}
C_2	6.2 JK^{-1}
α	10^{-4} VK^{-1}
C_∞	10 JK^{-1}
τ_c	0.1 s

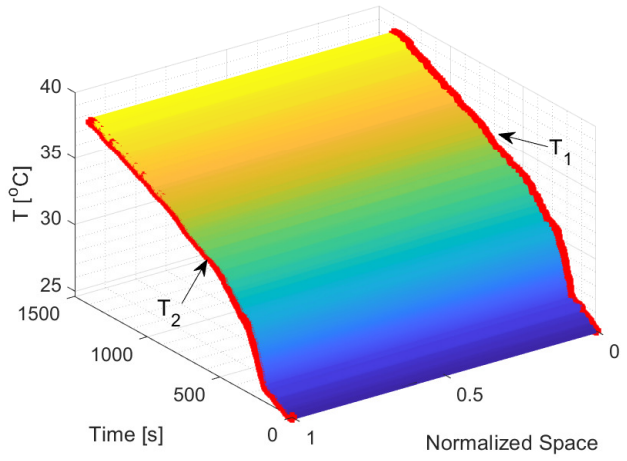

Fig. 3. Comparison between PDE plant model and the ODE design model.

B. Simulation Conditions

We have used the parameters shown in Table III for the simulation case studies. The value of internal electrical resistance R_s and entropic heat coefficient α are taken to be 0.05Ω and $10^{-4}VK^{-1}$, respectively. The simulation studies are performed in MATLAB R2022a. To take into account more realistic scenarios, we have added Gaussian noise $\mathcal{N}(\mu,\sigma^2) \equiv (0,1)$ in the measurement signals. To demonstrate the performance of the proposed controller, we show comparison with a battery cooled through natural convection. This comparison captures the most common situation of batteries where forced cooling is not available. A dynamic current profile generated based on the Urban Dynamometer Driving Schedule (UDDS) [17] is used in the simulation case studies, as shown in Fig. 4. We have obtained the control gains as $K_2 = 1.6887WK^{-1}$, $K_3 = -3.9391WK^{-1}$ by satisfying the design conditions (51), (52) and (53). The reference temperature is chosen as 25^oC for all the three temperature states and the unsafe region is considered to be beyond 50^oC. We inject a fault at $t = 500s$ which settles asymptotically to a certain value which varies depending on the location of the fault which can be the core or surface of the battery or both of them. These different fault scenarios are discussed in the subsequent case studies.

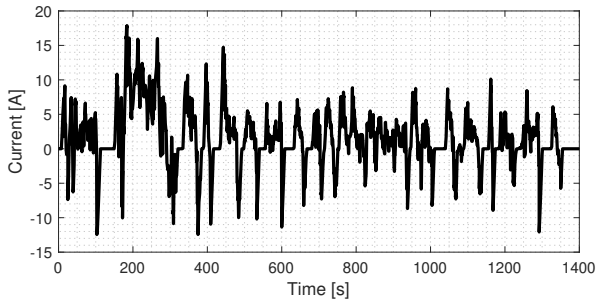

Fig. 4. Current profile based on UDDS.

C. Case Study 1: Performance under Thermal Fault at Core

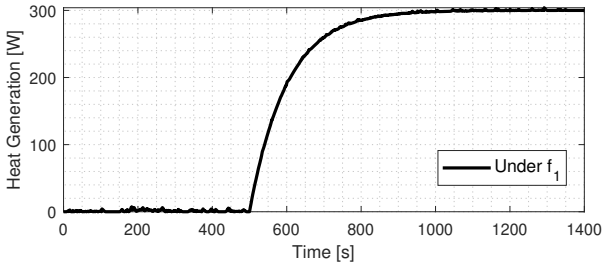

Fig. 5. Heat generation under internal fault.

In this case study, we discuss the performance of the controller when the thermal fault is present at the core of the battery. The fault is injected at $t = 500s$ magnitude of which settles asymptotically at $300W$. Since this corresponds to an internal fault, the effect of the fault gets directly reflected in the dynamics of the core temperature T_1 given by f_1 in (9).

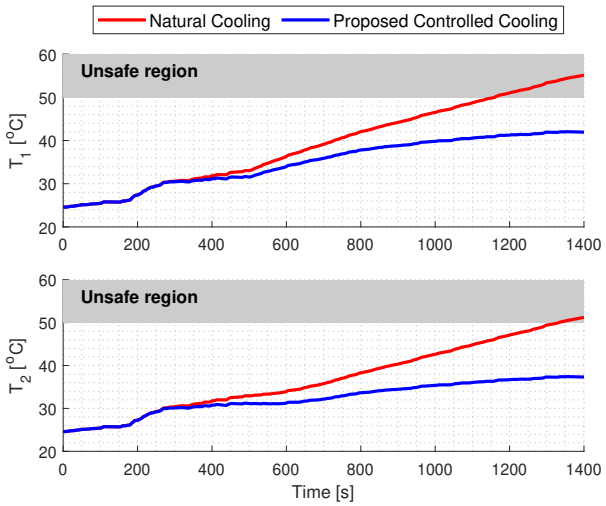

Fig. 6. Battery temperature's variation under internal fault.

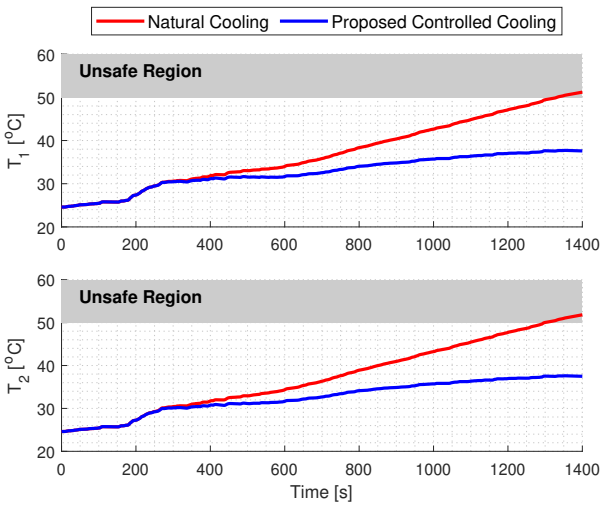

Fig. 8. Battery temperature's variation under external fault.

This effect is shown in Fig. 5. It can be seen from the Fig. 6 that as soon as the fault is injected, the temperatures T_1 and T_2 start increasing and natural cooling is unable to prevent the temperatures from entering the unsafe region whereas our proposed controller keeps the temperatures stable in the safe region. Hence, it can be said that the proposed approach performs better than the air cooling under internal faults. It is to be noted that since the fault is internal, the core temperature T_1 enters the unsafe region earlier than the surface temperature T_2 in case of natural cooling as is evident from Fig. 6.

D. Case Study 2: Performance under Thermal Fault at Surface

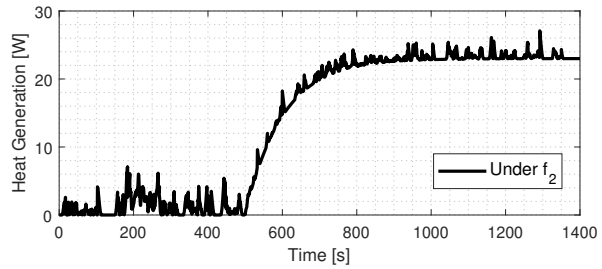

Fig. 7. Heat generation under external fault.

In this case study, we discuss the performance of the controller when the thermal fault is present at the surface of the battery. The fault is injected at $t = 500s$ magnitude of which settles asymptotically at $23W$. Since this corresponds to a external factor resulting in the fault, the effect of the fault gets directly reflected in the dynamics of the surface temperature T_2 given by f_2 in (10). This effect is shown in Fig. 7. It can be seen from the Fig. 8 that from the onset of fault injection, the temperatures T_1 and T_2 start increasing and natural cooling cannot keep the temperatures from going into the unsafe region whereas our proposed controller stabilizes the temperatures in the safe region. Hence, it can be said that the proposed approach performs better than the air cooling under surface faults also. It is to be noted that since the fault is external, it takes longer for the core temperature T_1 to enter the unsafe region in case of natural cooling as is evident from Fig. 8 whereas the surface temperature shows similar behavior as observed in Case Study 1.

E. Case Study 3: Performance under Thermal Fault at both, Core and Surface

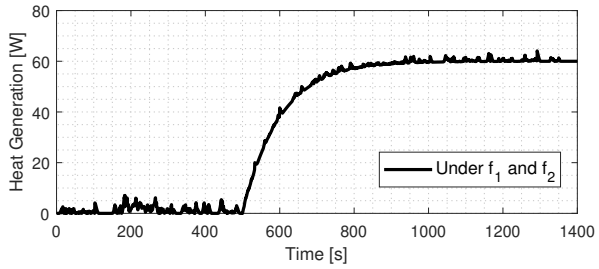

Fig. 9. Heat generation under internal and external faults.

In this case study, we discuss the performance of the controller when the thermal fault is present at both, the core and the surface of the battery. The faults are injected at $t = 500s$ magnitude of which settles asymptotically at $30W$. Since this corresponds to both, an internal and an external fault, the effect of the fault gets directly reflected in the dynamics of both, the core temperature T_1 given by f_1 in (9) and the surface temperature T_2 given by f_2 in (10). This effect is shown in Fig. 9. It can be seen from Fig. 10 that the temperatures T_1 and T_2 start increasing once the faults are injected and natural cooling cannot contain the temperatures in the safe region whereas our proposed controller is indeed able to stabilize the temperatures in the safe region. Hence, it can be said that under simultaneous fault scenario, the proposed approach performs better than the air cooling. It is to be noted that since both the faults are present, in case of natural cooling, the temperatures T_1 and T_2 enter the unsafe region much earlier as compared to Case Studies 1 and 2 as is evident from Fig. 6.

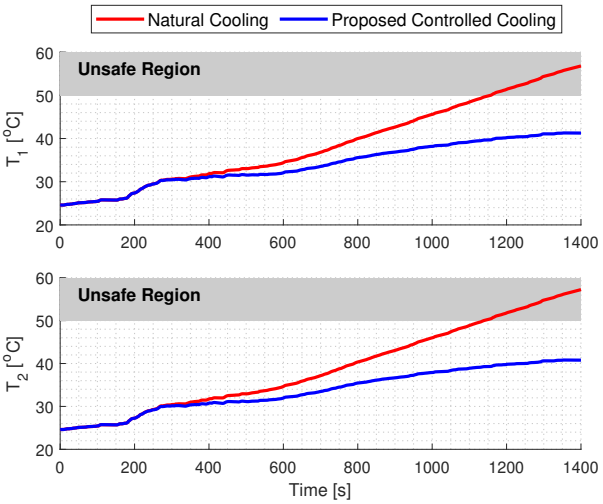

Fig. 10. Battery temperature's variation under both, internal and external faults.

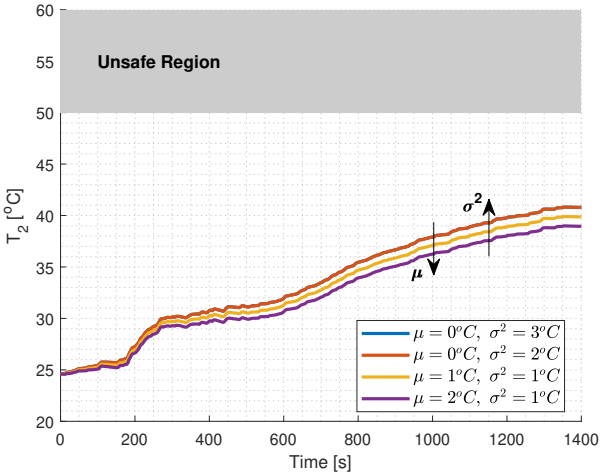

Fig. 12. Variation of the surface temperature T_2 with respect to the measurement noise.

F. Case Study 4: Performance under Measurement Noise

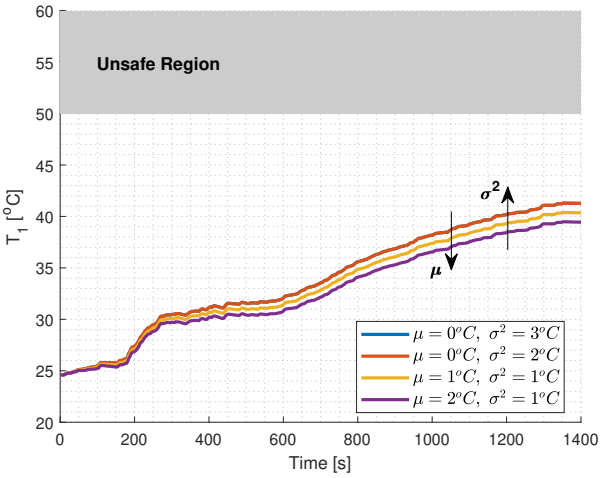

Fig. 11. Variation of the core temperature T_1 with respect to the measurement noise.

In this case study, we discuss the performance of the controller with respect to the variation in the measurement noise when the thermal fault is present at both, the core and the surface of the batter. The nature of the faults used in this Case Study correspond to those described in Case Study 3. We consider 4 scenarios of measurement noise where we either increase the bias μ or the variance σ^2 of the signals as compared to the Gaussian noise $\mathcal{N}(\mu, \sigma^2) \equiv (0, 1)$ used in the earlier case studies. It can be seen from Fig. 11 and Fig. 12 that increasing the bias μ from 0^oC to 2^oC reduces the temperatures T_1 and T_2 whereas increasing the variance σ^2 from 1^oC to 3^oC increases the temperatures T_1 and T_2. This effect is due to sensitivity of our approach with respect to the measurement noise. Essentially, this refers to the fact that our controlled cooling power responds better to the changing bias in the noise as opposed to changing variance. But with the shown variation in the measurement noise, our proposed approach is successful in keeping the temperatures stable in the safe region.

G. Case Study 5: Performance under Plant Parametric Uncertainties

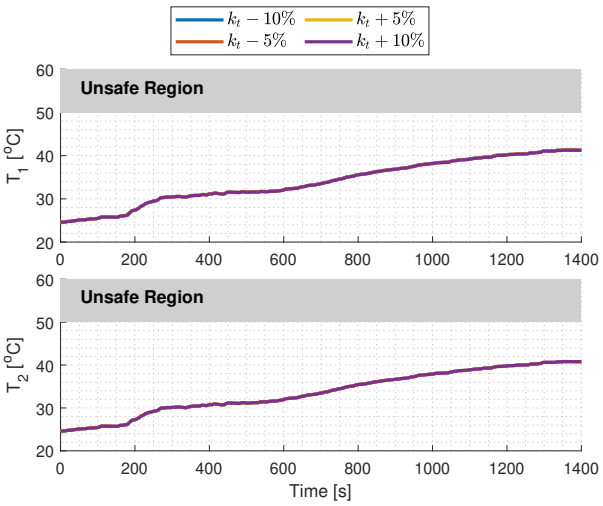

Fig. 13. Battery temperature's variation under uncertainties in battery thermal conductivity K_t.

In this case study, we discuss the performance of the controller with respect to the parametric uncertainties. Oftentimes, there is a mismatch between the plat parameters and the model parameters used for control design. We capture such parametric mismatch by introducing deviations in the PDE plant model parameters. The goal is to understand how the proposed control performs when such inaccuracies are present. We use the same scenario presented in Case Study 3 to illustrate this effect. We have considered uncertainties in battery thermal conductivity K_t, battery specific heat capacity C_p and convection heat transfer coefficient h. Four different magnitudes of uncertainties in each of the three parameters

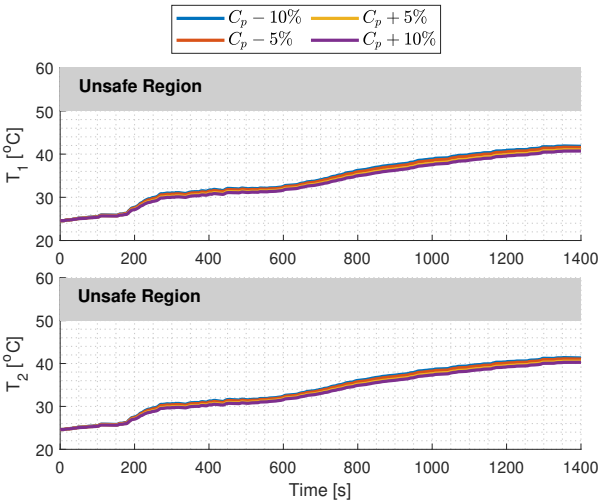

Fig. 14. Battery temperature's variation under uncertainties in battery specific heat capacity C_p.

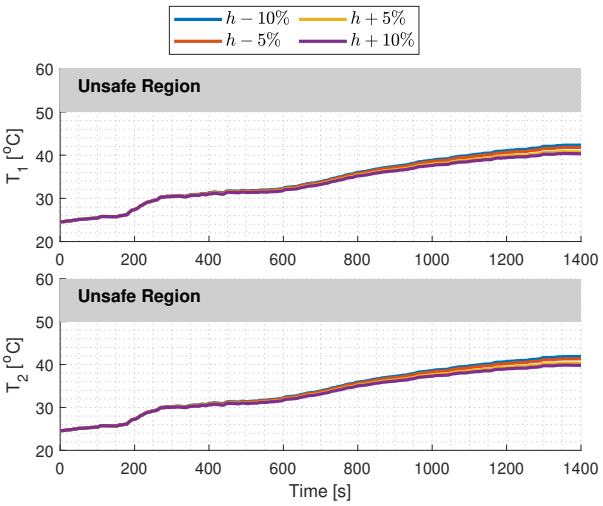

Fig. 15. Battery temperature's variation under uncertainties in convection heat transfer coefficient h.

K_t, C_p and h as $K_t \pm 5\%, \pm 10\%$, $C_p \pm 5\%, \pm 10\%$ and $h \pm 5\%, \pm 10\%$, respectively. It can be seen from Fig. 13 that our proposed controller is robust to the uncertainties in K_t whereas it is little sensitive to the uncertainties in C_p and h, as is evident from Figures 14 and 15, respectively. Qualitatively, this can be explained using the fact that the control action is at the surface. So, changing the convection heat transfer coefficient h has direct effect on cooling the surface of the battery and this effect is reflected in the core temperature too and hence the performance of the our controller is sensitive to the h uncertainties. In case of C_p and h, the final temperature values are little different from the ones under no uncertainties. However, none of these violated the safety limits. Accordingly, we can argue that the proposed control performs reasonably well when the parameter uncertainties are less than 10%.

V. Conclusions

This paper is an extension of our work published in [26]. Here, we have proposed a thermal fault-tolerant control algorithm for Lithium-ion batteries. Essentially, the control objective is to maintain the battery temperatures stable in the safe operating range under the presence of thermal faults. In addition the difference between the battery core and surface temperatures should not exceed a certain threshold. The problem is formulated as to design a control law in order to achieve the aforementioned control objectives. Particularly, we have utilized the input-to-state safety approach and combined it with the closed loop stability constraint to design the control gain matrix. The limit on the actual available cooling power is also taken into account. The applicability of the proposed framework is validated through the simulation case studies presented in Section IV. It is found that the control gains designed through the algorithm are indeed able to stabilize the temperatures in the safe limits under the presence of faults, noise in the measurement signals, unmodelled dynamics and parametric uncertainties of the plant.

References

[1] D. Lisbona and T. Snee, "A review of hazards associated with primary lithium and lithium-ion batteries," *Process Safety and Environmental Protection*, vol. 89, no. 6, pp. 434–442, 2011.

[2] S. Abada, G. Marlair, A. Lecocq, M. Petit, V. Sauvant-Moynot, and F. Huet, "Safety focused modeling of lithium-ion batteries: A review," *Journal of Power Sources*, vol. 306, pp. 178–192, Feb. 2016.

[3] A. Sidhu, A. Izadian, and S. Anwar, "Adaptive nonlinear model-based fault diagnosis of li-ion batteries," *IEEE Transactions on Industrial Electronics*, vol. 62, no. 2, pp. 1002–1011, 2014.

[4] Q. Yu, C. Wan, J. Li, R. Xiong, and Z. Chen, "A model-based sensor fault diagnosis scheme for batteries in electric vehicles," *Energies*, vol. 14, no. 4, p. 829, 2021.

[5] H. Chunhua, H. Ren, W. Runcai, and Y. Jianbo, "Fault prediction and fault-tolerant of lithium-ion batteries temperature failure for electric vehicle," in *2012 Third International Conference on Digital Manufacturing & Automation*. IEEE, 2012, pp. 410–413.

[6] S. Dey, Z. A. Biron, S. Tatipamula, N. Das, S. Mohon, B. Ayalew, and P. Pisu, "Model-based real-time thermal fault diagnosis of lithium-ion batteries," *Control Engineering Practice*, vol. 56, pp. 37–48, 2016.

[7] Q. Lin, J. Wang, R. Xiong, W. Shen, and H. He, "Towards a smarter battery management system: A critical review on optimal charging methods of lithium ion batteries," *Energy*, vol. 183, pp. 220–234, 2019.

[8] K. A. Smith, C. D. Rahn, and C.-Y. Wang, "Model-based electrochemical estimation and constraint management for pulse operation of lithium ion batteries," *IEEE Transactions on Control Systems Technology*, vol. 18, no. 3, pp. 654–663, 2009.

[9] H. Perez, N. Shahmohammadhamedani, and S. Moura, "Enhanced performance of li-ion batteries via modified reference governors and electrochemical models," *IEEE/ASME Transactions on Mechatronics*, vol. 20, no. 4, pp. 1511–1520, 2015.

[10] F. Altaf, B. Egardt, and L. J. Mårdh, "Load management of modular battery using model predictive control: Thermal and state-of-charge balancing," *IEEE Transactions on Control Systems Technology*, vol. 25, no. 1, pp. 47–62, 2016.

[11] E. Kim, K. G. Shin, and J. Lee, "Real-time battery thermal management for electric vehicles," in *2014 ACM/IEEE International Conference on Cyber-Physical Systems (ICCPS)*. IEEE, 2014, pp. 72–83.

[12] X. Tao and J. Wagner, "A thermal management system for the battery pack of a hybrid electric vehicle: modeling and control," *Proceedings of the Institution of Mechanical Engineers, Part D: Journal of Automobile Engineering*, vol. 230, no. 2, pp. 190–201, 2016.

[13] Y. Chung and M. S. Kim, "Thermal analysis and pack level design of battery thermal management system with liquid cooling for electric vehicles," *Energy Conversion and Management*, vol. 196, pp. 105–116, 2019.

[14] G. Karimi and X. Li, "Thermal management of lithium-ion batteries for electric vehicles," *International Journal of Energy Research*, vol. 37, no. 1, pp. 13–24, 2013.

[15] L. Seybold, M. Witczak, P. Majdzik, and R. Stetter, "Towards robust predictive fault-tolerant control for a battery assembly system," *International Journal of Applied Mathematics and Computer Science*, vol. 25, no. 4, pp. 849–862, 2015.

[16] R. Xiong, Q. Yu, and W. Shen, "Review on sensors fault diagnosis and fault-tolerant techniques for lithium ion batteries in electric vehicles," in *2018 13th IEEE Conference on Industrial Electronics and Applications (ICIEA)*. IEEE, 2018, pp. 406–410.

[17] S. Dey, Y. Shi, K. Smith, and M. Khanra, "Safer batteries via active fault tolerant control," in *2019 American Control Conference (ACC)*. IEEE, 2019, pp. 1561–1566.

[18] J. Jiang and X. Yu, "Fault-tolerant control systems: A comparative study between active and passive approaches," *Annual Reviews in Control*, vol. 36, no. 1, pp. 60–72, 2012.

[19] P. Wieland and F. Allgöwer, "Constructive safety using control barrier functions," *IFAC Proceedings Volumes*, vol. 40, no. 12, pp. 462–467, 2007.

[20] S. Kolathaya and A. D. Ames, "Input-to-state safety with control barrier functions," *IEEE Control Systems Letters*, vol. 3, no. 1, pp. 108–113, 2018.

[21] X. Xu, P. Tabuada, J. W. Grizzle, and A. D. Ames, "Robustness of control barrier functions for safety critical control," *IFAC-PapersOnLine*, vol. 48, no. 27, pp. 54–61, 2015.

[22] A. Taylor, A. Singletary, Y. Yue, and A. Ames, "Learning for safety-critical control with control barrier functions," in *Learning for Dynamics and Control*. PMLR, 2020, pp. 708–717.

[23] M. Z. Romdlony and B. Jayawardhana, "On the new notion of input-to-state safety," in *2016 IEEE 55th Conference on Decision and Control (CDC)*. IEEE, 2016, pp. 6403–6409.

[24] M. Romdlony and B. Jayawardhana, "Stabilization with guaranteed safety using control lyapunov–barrier function," *Automatica*, vol. 66, pp. 39–47, 2016.

[25] T. Roy, A. Knichel, and S. Dey, "An input-to-state safety approach to anomaly-resilient parabolic pdes: Application to cyber-physical battery modules," *arXiv preprint arXiv:2201.02239*, 2022.

[26] S. D. Vyas, T. Roy, and S. Dey, "Thermal fault-tolerance in lithium-ion battery cells: A barrier function based input-to-state safety framework," in *2022 IEEE Conference on Control Technology and Applications (CCTA)*, 2022, pp. 1178–1183.

[27] C. Park and A. K. Jaura, "Dynamic thermal model of li-ion battery for predictive behavior in hybrid and fuel cell vehicles," SAE Technical Paper, Tech. Rep., 2003.

[28] X. Lin, H. E. Perez, S. Mohan, J. B. Siegel, A. G. Stefanopoulou, Y. Ding, and M. P. Castanier, "A lumped-parameter electro-thermal model for cylindrical batteries," *Journal of Power Sources*, vol. 257, pp. 1–11, 2014.

[29] H. Chan, "A new battery model for use with battery energy storage systems and electric vehicles power systems," in *2000 IEEE Power Engineering Society Winter Meeting. Conference Proceedings (Cat. No.00CH37077)*, vol. 1, 2000, pp. 470–475 vol.1.

[30] A. Seaman, T.-S. Dao, and J. McPhee, "A survey of mathematics-based equivalent-circuit and electrochemical battery models for hybrid and electric vehicle simulation," *Journal of Power Sources*, vol. 256, pp. 410–423, 2014.

[31] D. Bernardi, E. Pawlikowski, and J. Newman, "A general energy balance for battery systems," *Journal of The Electrochemical Society*, vol. 132, no. 1, p. 5, 1985.

[32] T. M. Bandhauer, S. Garimella, and T. F. Fuller, "A critical review of thermal issues in lithium-ion batteries," *Journal of The Electrochemical Society*, vol. 158, no. 3, p. R1, 2011.

[33] D. H. Doughty and E. P. Roth, "A general discussion of li ion battery safety," *The Electrochemical Society Interface*, vol. 21, no. 2, p. 37, 2012.

[34] C. Hendricks, N. Williard, S. Mathew, and M. Pecht, "A failure modes, mechanisms, and effects analysis (fmmea) of lithium-ion batteries," *Journal of Power Sources*, vol. 297, pp. 113–120, 2015.

[35] G. Dong and M. Lin, "Model-based thermal anomaly detection for lithium-ion batteries using multiple-model residual generation," *Journal of Energy Storage*, vol. 40, p. 102740, 2021.

[36] S. Dey, H. E. Perez, and S. J. Moura, "Model-based battery thermal fault diagnostics: Algorithms, analysis, and experiments," *IEEE Transactions on Control Systems Technology*, vol. 27, no. 2, pp. 576–587, 2019.

[37] J. Wei, G. Dong, and Z. Chen, "Lyapunov-based thermal fault diagnosis of cylindrical lithium-ion batteries," *IEEE Transactions on Industrial Electronics*, vol. 67, no. 6, pp. 4670–4679, 2019.

[38] S. Al Hallaj, H. Maleki, J.-S. Hong, and J. R. Selman, "Thermal modeling and design considerations of lithium-ion batteries," *Journal of Power Sources*, vol. 83, no. 1-2, pp. 1–8, 1999.